eChem
https://www.sciltp.com/journals/eChem



Article

Check for updates

Disposable Screen-Printed Ca^{2+} Sensor Using NH_2-MIL-125@rGO as Solid-Contact Layer for Raw Milk Analysis

Wanting Zhang [1], Yunrui Fang [1], Qingbo An [1,*], Zhongqian Song [2], Bin Cai [3], Jing Sun [1,*] and Li Niu [4,*]

[1] Jilin Provincial International Joint Research Center of Photo-Functional Materials and Chemistry, School of Chemistry & Environmental Engineering, Changchun University of Science and Technology, Changchun 130022, China
[2] College of Medical Information and Artificial Intelligence, Shandong First Medical University & Shandong Academy of Medical Sciences, Jinan 250117, China
[3] School of Chemistry and Chemical Engineering, Shandong University, Jinan 250100, China
[4] School of Chemical Engineering and Technology, Sun Yat-sen University, Zhuhai 519082, China
* Correspondence: qban@cust.edu.cn (Q.A.); sjcust@126.com (J.S.); niuli@mail.sysu.edu.cn (L.N.)

How To Cite: Zhang, W.; Fang, Y.; An, Q.; et al. Disposable Screen-Printed Ca^{2+} Sensor Using NH_2-MIL-125@rGO as Solid-Contact Layer for Raw Milk Analysis. *eChem* **2026**, *2*(2), 12. https://doi.org/10.53941/echem.2026.100012

Received: 30 June 2026
Revised: 3 September 2026
Accepted: 8 October 2026
Published: 26 October 2026

Abstract: Solid-contact ion-selective electrodes have been extensively utilized for calcium ion detection, particularly in applications involving milk samples. In this study, a solid-contact was developed using a composite material of $Ti_8O_8(OH)_4(H_2bdc\text{-}NH_2)_6$ (NH_2-MIL-125) and reduced graphene oxide (rGO) to prepare calcium SC-ISE (NH_2-MIL-125@rGO/Ca^{2+}-ISE). The NH_2-MIL-125@rGO/Ca^{2+}-ISE demonstrated high double-layer capacitance (222 μF) and rapid electron transfer capabilities. Within the calcium ion concentration range of 10^{-7}~10^{-1} M, the electrode exhibited an excellent Nernstian response, with a rapid response time (2~3 s) and a low detection limit of $10^{-7.2}$ M. Additionally, the electrode performed exceptionally in water layer and anti-interference tests, showing enhanced potential stability and response speed while being unaffected by environmental factors such as light, CO_2, and O_2. These results confirm the superior performance of the NH_2-MIL-125@rGO composite as a solid-contact layer, therefore constructed disposable screen-printed calcium potentiometric sensor. In particular, it demonstrated the capability for rapid and accurate analysis of calcium content in untreated milk samples, highlighting the significant practical potential for development of calibration-free SC-ISEs.

Keywords: metal-organic framework; solid contact; ion-selective electrode; ion sensor

1. Introduction

Calcium is the main component of human bones and teeth for children and adolescents. Sufficient calcium ions in milk can provide essential raw materials for growth and effectively prevent rickets and other bone dysplasia [1], thus calcium ion content is a core element for evaluating milk quality. So far, a variety of methods for the detection of calcium ions have been reported, such as atomic absorption spectrometry [2], atomic fluorescence spectrometry [3], redox titration, spectrophotometry [4]. However, these methods have their own limitations, spectrophotometer method is susceptible to the influence of sample composition inhomogeneity, resulting in low measurement precision. Although atomic absorption spectrometry is accurate, it requires expensive instrumentation and long detection cycles. Therefore, detection methods with low cost, simple operation and high sensitivity are highly demanded.

Solid-contact ion-selective electrodes (SC-ISEs) is an ideal alternative, which are characterized by fast response time, high sensitivity, excellent selectivity, and good reproducibility. They have been widely used in biological and environmental analysis. In addition, the easy miniaturization, convenient storage and portability of SC-ISEs successfully solve the leakage problem of internal reference solution in traditional liquid-contact

Copyright: © 2026 by the authors. This is an open access article under the terms and conditions of the Creative Commons Attribution (CC BY) license (https://creativecommons.org/licenses/by/4.0/).
Publisher's Note: Scilight stays neutral with regard to jurisdictional claims in published maps and institutional affiliations.

electrodes. SC-ISEs uses ion selective membrane to selectively respond to a specific ion. When measuring solution containing the ions, a membrane potential is generated at the interface between the sensitive membrane and the solution that is directly related to ion activity. In order to improve the detection range and maintain the stability of potential, a solid-contact layer (SC) is introduced between the conductive substrate and the ion selective membrane to increase the ion-to-electron transduction capability. The large interfacial capacitance of the SC and the resistance of the water layer are two key factors to reduce the potential drift of SC-ISE [5,6].

Until now, widely used solid contact materials include conductive polymers [7,8], carbon materials [9–12], redox molecular pairs [13,14], and noble metal nanoparticles [15], metal-organic frameworks (MOFs) [16,17], and MXene nanosheets [18]. Among them, MOFs as a kind of porous crystal material, have attracted more and more attention because of their unique advantages, such as easy synthesis, structural diversity, large specific surface area, high porosity and good chemical stability [19,20]. Nevertheless, most MOFs suffer from poor electrical conductivity, restricting their application as SC. In order to overcome this problem, some modification strategies are needed to improve the conductivity of MOFs. Benefiting from the tunable central metal ions and peripheral ligands of MOFs, material properties can be optimized via selective modification [21].Graphene has advantages such as high specific surface area, electrical conductivity and chemical stability, which can provide supports for MOFs, enhance the overall mechanical stability of the composite, and the presence of the metal-organic framework can effectively separate the graphene sheets and prevent them from agglomerating, thus maintaining the high specific surface area of MOFs graphene composites.

In this work, MOF @reduced graphene oxide composites (NH_2-MIL-125@rGO) were prepared by a solvothermal method as SC. Through the synergistic interaction between the two, the composite not only makes up for the lack of electrical conductivity of the MOF material, but also improves the limitation of the porosity of graphene, making the composite show excellent large double layer capacitance, fast electron transduction ability and good hydrophobicity. When the graphene oxide (GO) mass fraction is 13%, the electrode capacitance performance reaches the best state. NH_2-MIL-125@rGO electrochemical sensors made of solid contact materials can effectively prevent the formation of a water layer between the electrode and the film interface, significantly reducing the interfacial resistance. This characteristic makes the sensor show good reproducibility and stability in the detection of calcium ions. Therefore, the disposable screen printed electrode was prepared and successfully applied to the rapid detection of Ca^{2+} content in milk samples, which provides convenience for the detection of calcium ions in actual milk samples.

2. Experimental Section

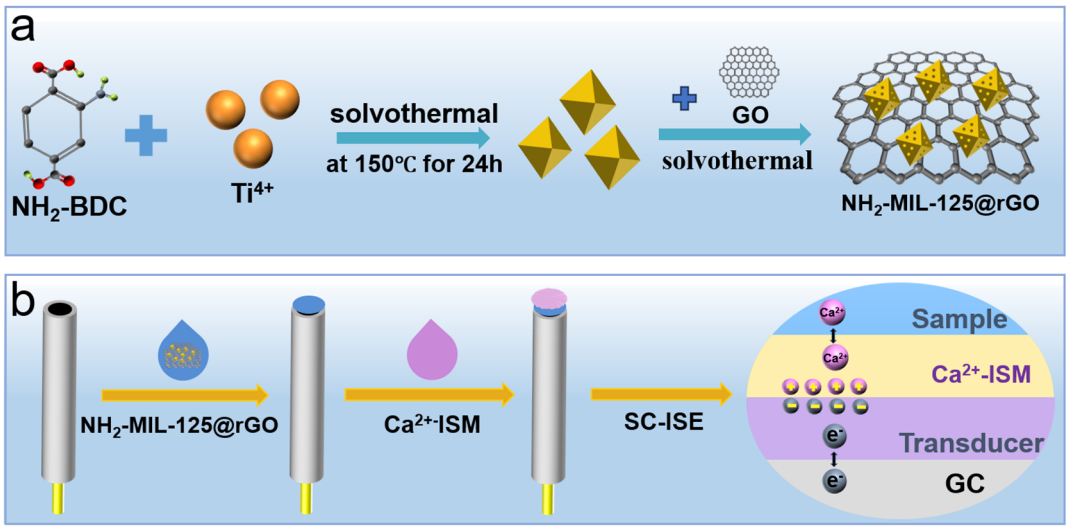
2.1. Reagents and Materials

Tetrabutyl titanate (TPOT), 2-amino-terephthalic acid (NH_2-BDC, 98%), N, n-dimethylformamide, tetra [3,5-bis (trifluoromethyl) phenyl] sodium borate (NaTFPB), hydrogen peroxide (30%), methanol, acetic acid and ethanol were purchased from Aladdin (Shanghai, China). Concentrated nitric acid, concentrated sulfuric acid, potassium chloride (KCl), ferric chloride ($FeCl_3$), sodium chloride (NaCl), magnesium chloride ($MgCl_2$), calcium chloride ($CaCl_2$), barium chloride ($BaCl_2$), copper chloride ($CuCl_2$), potassium permanganate were purchased from Sigma-Aldrich (St. Louis, MO, USA). Calcium ion carrier N, n-dicyclohexyl-2-[2-(dicyclohexylamino)-2-oxyethoxy] acetamide (ETH-129), 2-nitrophenyl octylether (σ-NPOE), high molecular weight polyvinyl chloride (PVC), tetrahydrofuran (THF) were purchased from Fluka (Buchs, Switzerland). Graphene (Supplementary Materials). Aqueous solutions were prepared with freshly deionized water (18.2 MΩ cm specific resistance). The disposable carbon screen printed electrodes were purchased from Qingdao Poten Technology Co. (Qingdao, China).

2.2. Preparation of NH_2-MIL-125@rGO Transducer

According to the previously reported literature [22], NH_2-MIL-125 and NH_2-MIL-125@rGO composites were synthesized by solvothermal synthesis. First, 0.15 mL TPOT and 0.14 g NH_2-BDC were dissolved in a mixed solution of 9 mL DMF and 1 mL methanol, and then 0.53 mL acetic acid was added to the solution and stirred to fully dissolve it. Then the mixture was transferred to a 50 mL polytetrafluoroethylene autoclave and reacted at 150 °C for 24 h. After the reaction, it was cooled to room temperature, washed with deionized water, methanol and deionized water in turn, and freeze-dried to obtain a yellow solid powder.

The synthesis method of NH_2-MIL-125@rGO composite material is similar to the above process. A certain amount of NH_2-MIL-125 is weighed to prepare an aqueous solution, and different mass fractions of GO dispersion are added. The two solutions are mixed and stirred for 30 min, and then transferred to a 50 mL high-pressure reactor for hydrothermal reduction reaction at 120 °C for 8 h. After freeze-drying, a black sample NH_2-MIL-125@rGO is obtained (Scheme 1a).



Scheme 1. The illustrations for (**a**) the preparation of NH_2-MIL-125@rGO composites and (**b**) the fabrication of SC-ISE for Ca^{2+} detection.

2.3. Preparation of SC-Ca^{2+}-ISEs

The glassy carbon electrodes were polished with fine alumina powders (0.3 and 0.05 μm) on a polishing cloth, and then cleaned by alternating ultrasonication with ultrapure water and ethanol. Configured NH_2-MIL-125 and NH_2-MIL-125@rGO dispersions were dripped onto the surface of the polished GC electrodes, which were air-dried under nitrogen purge, and then a 20 μL drop of Ca^{2+} selective membrane (Ca^{2+}-ISM) was placed on the top of the electrode (Scheme 1b). The Ca^{2+}-ISM component containing 0.46 wt% calcium ionophore II (ETH 129), 0.48 wt% NaTFPB, 33.02 wt% PVC and 66.04 wt% *σ*-NPOE (totally 360 mg). Dissolve in 1.8 mL THF to obtain a membrane cocktail solution [23]. For comparison three kinds of electrodes, Ca^{2+}-ISE, NH_2-MIL-125/Ca^{2+}-ISE and NH_2-MIL-125@rGO/Ca^{2+}-ISE were prepared and dried overnight.

The preparation process of the disposable solid-state screen-printed electrode is the same as the above process, except that the working electrode of SPE is selected as the substrate.

2.4. Electrochemical Measurements

All electrochemical evaluations are performed using the CHI760E Electrochemical workstation with a typical three-electrode system. NH_2-MIL-125@rGO/Ca^{2+}-ISE, Ag/AgCl electrode and Pt wire are used as working electrode, reference electrode and counter electrode, respectively. The impedance spectrum was recorded in a 0.1 M $CaCl_2$ solution with a frequency range of 10^{-6}~10^{-1} Hz and an amplitude of 100 mV. Chronopotentiometry was performed by continuously applying a constant current of ±1 nA for 60 s in a 0.1 M $CaCl_2$ solution, and the electrodes were adjusted in 1 mM $CaCl_2$ overnight prior to chronopotentiometry.

3. Results and Discussion

As shown in Figure 1a,b, the NH_2-MIL-125@rGO composites were investigated by scanning electron microscopy (SEM). The octahedral and cubic structures of NH_2-MIL-125 crystals are clearly shown in the image, with average side lengths in the range of 1–1.2 μm. This morphological feature is highly consistent with the NH_2-MIL-125 frame morphology recorded in previous literature [24]. Figure 1c,d exhibits the surface topography of NH_2-MIL-125@rGO composite, NH_2-MIL-125 crystals can be observed attached to the surface of rGO in the form of regular nanoparticles. Further, TEM characterization also revealed the detailed microstructure of the material, as shown in Figure S9, where the three-dimensional structure of NH_2-MIL-125 and the typical lamellar structure of rGO were observed. The results showed that rGO was well combined with NH_2-MIL-125.

The XRD patterns of the prepared GO, NH_2-MIL-125 and NH_2-MIL-125@rGO composites are depicted in Figure 1e. NH_2-MIL-125 exhibits a typical inorganic crystal structure, a finding that is highly consistent with previous reports [25]. In the XRD pattern of GO, a sharp diffraction peak at 10° is clearly observed, which corresponds perfectly to the (001) diffraction peak of the hexagonal structure of graphite [26]. For the composite NH_2-MIL-125@rGO, the GO to rGO conversion process is accompanied by functional group change, which is a typical characteristic of amorphous carbon or graphene structure in rGO samples. The peak of the composite NH_2-

MIL-125@rGO sample is significantly shifted to a lower angle than that of pure NH_2-MIL-125, indicating that the composite is well bonded [27]. However, the diffraction peak of rGO is not obvious, which may be due to the low content of rGO [28]. In addition, the XRD pattern at NH_2-MIL-125@rGO further reveals that the introduction of rGO does not cause any damage to the crystal structure of NH_2-MIL-125.

Raman measurements of GO, rGO and NH_2-MIL-125@rGO were carried out to assess the structural disorder of the as-prepared composites. The structural and chemical features of the composites can be reflected by the position and intensity of characteristic peaks in Figure 1f. The D band is associated with defect induced vibrational modes of sp^2 carbon structures, particularly the breathing modes of sp^2 carbon rings, whereas the G band originates from the in-plane stretching vibrations of sp^2 bonded carbon atoms. The intensity ratio (I_D/I_G) is commonly used to quantify the disorder and defect density within graphene based materials, which strongly influences the conductive performance of composites [29]. Generally, a larger (I_D/I_G) value indicates higher defect content and greater structural disorder. The ratios for GO, rGO and NH_2-MIL-125@rGO are 0.89, 1.16, and 1.05 respectively. The increase after GO reduction may reflect changes in the carbon structure associated with the removal of oxygen-containing groups, while the subsequent decrease in the composite suggests further structural modification during composite formation [30]. The electrical transport properties were further evaluated by electrochemical impedance spectroscopy.

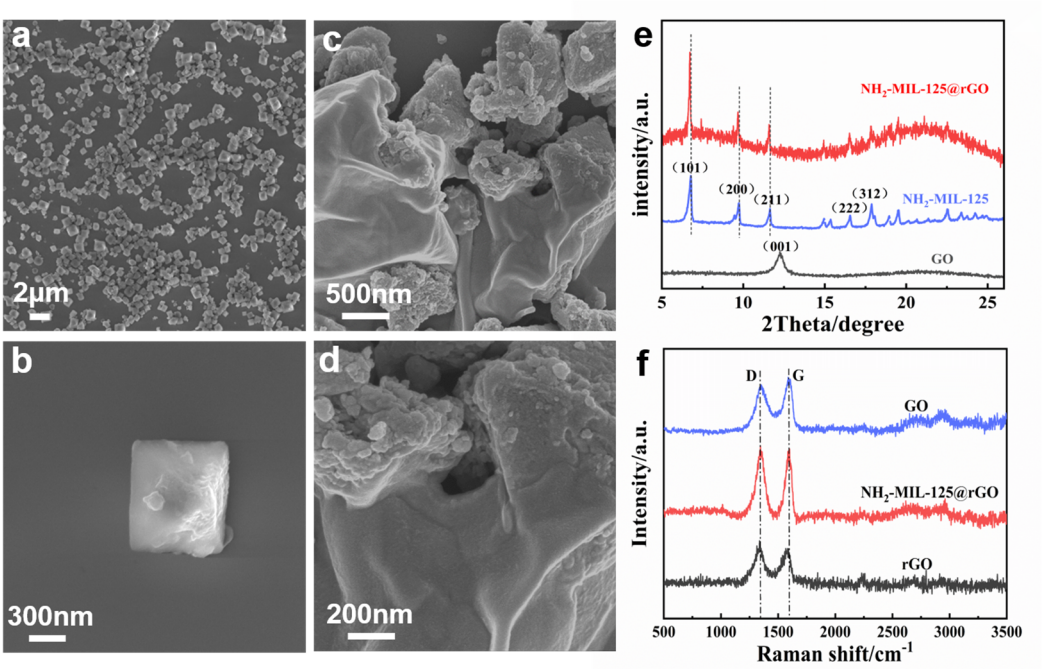


Figure 1. SEM images of (**a**,**b**) NH_2-MIL-125 and (**c**,**d**) NH_2-MIL-125@rGO composites. (**e**) XRD and (**f**) Raman spectra of GO, rGO and NH_2-MIL-125@rGO.

The XPS spectra were employed for the elemental composition analyses of NH_2-MIL-125 and NH_2-MIL-125@rGO composites, as shown in Figure 2. The XPS data showed that Ti, O, C and N elements exist in the composite, and there are two main peaks at 285.3 and 530.7 eV, namely C 1s and O 1s, respectively. The carbon content of NH_2-MIL-125@rGO is higher than that of NH_2-MIL-125, which confirms that NH_2-MIL-125 contains rGO, indicating that the material is well composite [31]. Figure 2c demonstrates the symmetric peaks of $Ti2p_{3/2}$ and $Ti2p_{1/2}$ at 458.8 eV and 464.2 eV in the Ti2p spectrum, indicating that the oxygen-bound titanium in the Ti-oxygen cluster maintains an IV oxidation state [32]. Unexpectedly, the characteristic peak of Ti shifted after the introduction of rGO, which may be due to the formation of the Ti-O-C bond (Figure 2f). The C 1s spectrum of NH_2-MIL-125 can be deconvoluted into three peaks at 284.56, 286.05, and 288.54 eV, which are assigned to C=C/C–C, C–O/C–OH, and C=O species, respectively (Figure 2b). The O 1s spectrum was further analyzed to uncover the interfacial interaction and its influence on electrical conductivity. The shift of the O 1s peak upon rGO incorporation arises from the formation of Ti-O-C covalent bonds between NH_2-MIL-125 and rGO. Such covalent linkage induces strong interfacial electronic coupling, accelerates interfacial charge transfer and reduces interfacial resistance, therefore facilitating electron transport and contributing to the improved conductivity of the NH_2-MIL-125 @rGO composite.

At the same time, the spectra of O 1s and N 1s (Figure S3) further indicate that there may be an interaction between NH_2-MIL-125@rGO.

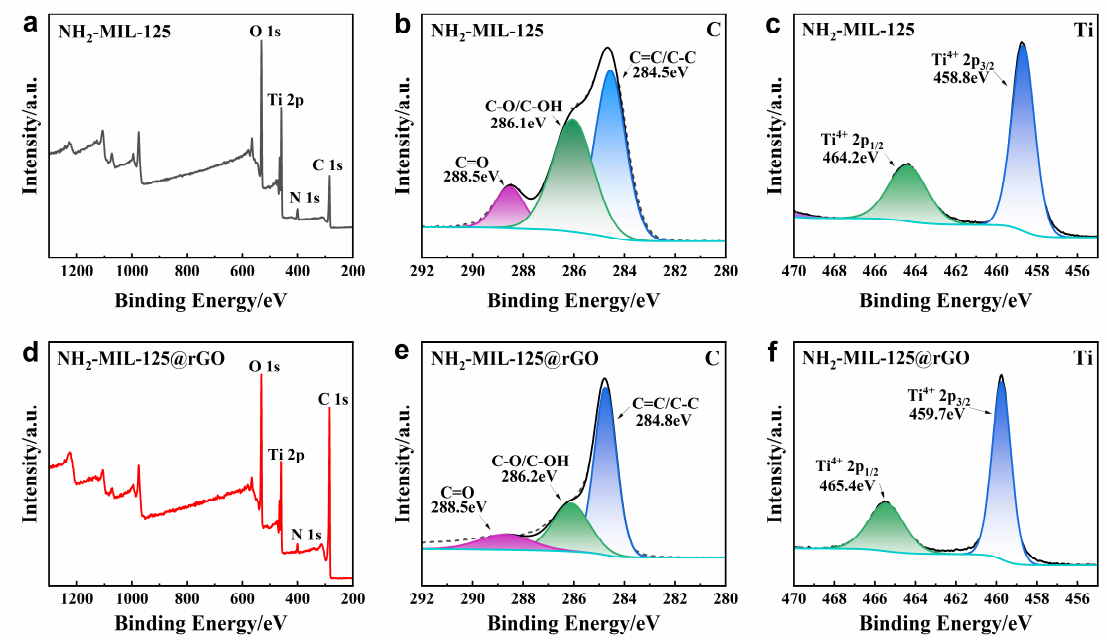


Figure 2. (**a**) XPS spectra of NH_2-MIL-125 and (**b**,**c**) XPS spectra of C 1s and Ti 2p at NH_2-MIL-125; (**d**) XPS spectra of NH_2-MIL-125@rGO and (**e**,**f**) XPS spectra of C 1s and Ti 2p for NH_2-MIL-125@rGO.

The electrochemical properties of GC and GC coated with different materials were studied by CV and EIS in 0.1 M $CaCl_2$ solution. In particular, the NH_2-MIL-125@rGO/Ca^{2+}-ISE exhibits a higher capacitance current than the NH_2-MIL-125/Ca^{2+}-ISE and unmodified bare GC electrodes. This phenomenon showed that by introducing rGO, the double-layer capacitive performance of the electrode can be effectively improved, as shown in Figure 3a. In order to better understand the effect of rGO content on the capacitive performance of NH_2-MIL-125@rGO/Ca^{2+}-ISE, a systematic study was carried out (Figure 3b). The results showed that when the content of rGO reached 13 wt%, the capacitive current of the electrode increased significantly. This may be due to some structural synergy occurring between rGO and NH_2-MIL-125 at this content, which facilitates charge storage and transfer. However, when the rGO content is further increased to 17 wt% and above, the capacitance current shows a gradually decreasing trend. This may be due to excessive rGO causing aggregation and stacking between materials, which in turn increases the internal resistance of the electrode, hindering the transfer and storage of charge.

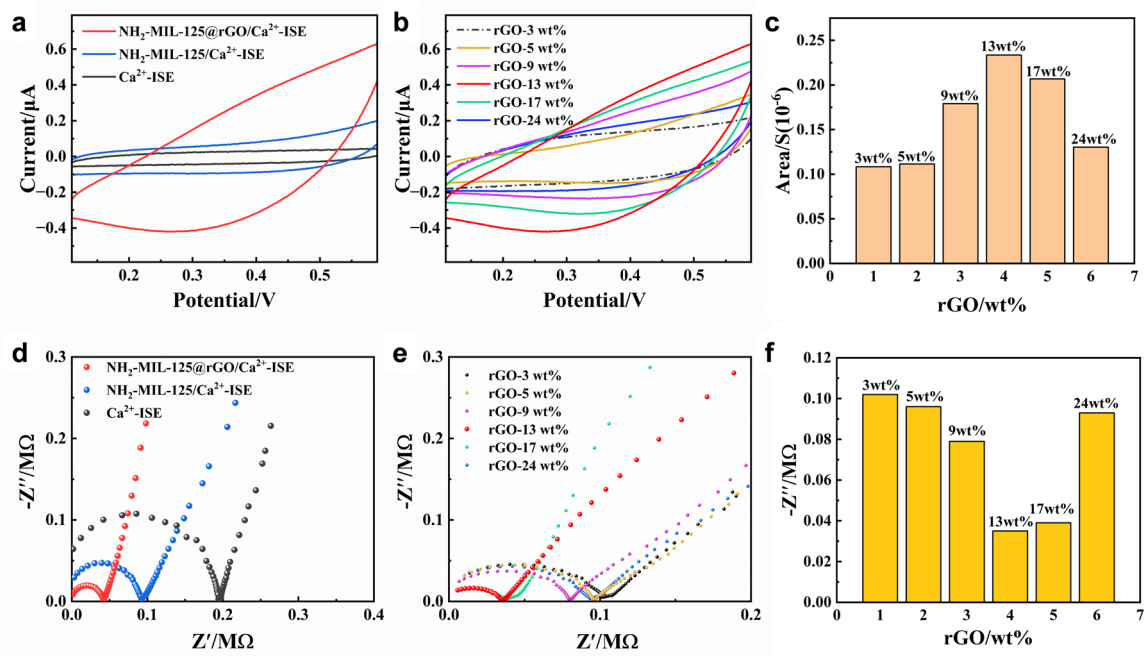


Figure 3. (**a**) cyclic voltammetry curves of Ca^{2+}-ISE, NH_2-MIL-125/Ca^{2+}-ISE and NH_2-MIL-125@rGO/Ca^{2+}-ISE; (**b**) Cyclic voltammetry test curves of NH_2-MIL-125@rGO/Ca^{2+}-ISE electrodes with different ratios of rGO; (**c**) The

peak areas corresponding to rGO with different mass fractions; (**d**) Impedance spectra of Ca^{2+}-ISE, NH_2-MIL-125/Ca^{2+}-ISE and NH_2-MIL125@rGO/Ca^{2+}-ISE; (**e**) Impedance spectra of NH_2-MIL125@rGO/Ca^{2+}-ISE electrodes with different ratios of rGO; (**f**) The resistance values corresponding to rGO with different mass fractions.

To further verify the ion electron transduction ability and capacitance of SC, electrochemical impedance spectroscopy (EIS) experiment was carried out, and the impedance diagram was displayed [33,34] (Figure S4). By analysis via a Z View software, fitted electrochemical parameters are summarized in Table S3. In the high frequency region, the semicircle diameter represents the bulk resistance of the membrane and the contact resistance between the membrane and the SC layer [35]. The bulk resistance Rb decreases from 0.08 MΩ to about 0.045 MΩ (Figure 3d), indicating that the introduction of NH_2-MIL-125@rGO between the GC substrate and the Ca^{2+}-ISM can effectively reduce the contact impedance and promote the transport of charges at the interface, thus having excellent conductivity. In the low frequency region, it is caused by the coupling of double-layer capacitance and charge transfer resistance at the buried interface between the ISM and the underlying conductor. As shown in Figure 3e, the rGO content of 13 wt% shows a smaller high-frequency semicircle, indicating a larger high-frequency capacitance and a smaller charge-transfer resistance. These results show that NH_2-MIL-125@rGO-13 wt% as a transduction layer can reduce electron transport resistance, promote charge transfer rate, and improve the stability of electrode potential during potential response. Therefore, NH_2-MIL-125@rGO electrode containing 13 wt% rGO was chosen for subsequent experiments. EIS measurement results showed that the addition of SC layer significantly increases the capacitance of the sensor and makes the response of the sensor more stable. Similar to the results obtained for CV, NH_2-MIL-125@rGO composite electrode has the largest capacitance, and the obtained capacitance values are slightly different, which may be due to differences in electrochemical techniques [36]. The electrical conductivity of GO and rGO was also investigated through EIS experiments (Figure S4b). The results showed that the low-frequency impedance of rGO was significantly lower than that of GO, indicating that reducing GO to rGO can enhance the electrical conductivity of the material.

The capacitance is studied. The transduction mechanism of the NH_2-MIL-125@rGO SC-ISE is based on double-layer capacitance at the SC/ISE interface [10]. As shown in Figure 4, there are three interfaces, namely GC/SC, SC/ISM, and ISM/sample solution, NH_2-MIL-125@rGO can be compared to an asymmetric capacitor, with one side is formed by electronic charges in NH_2-MIL-125@rGO and the other side s formed by cations in the ISM. Among them, ISM plays the role of calcium ion recognition, NH_2-MIL-125@rGO has the ability to converting ion signals into electrical potential signals. Therefore, capacitance is the decisive factor to maintain the potential stability of SC-ISEs.

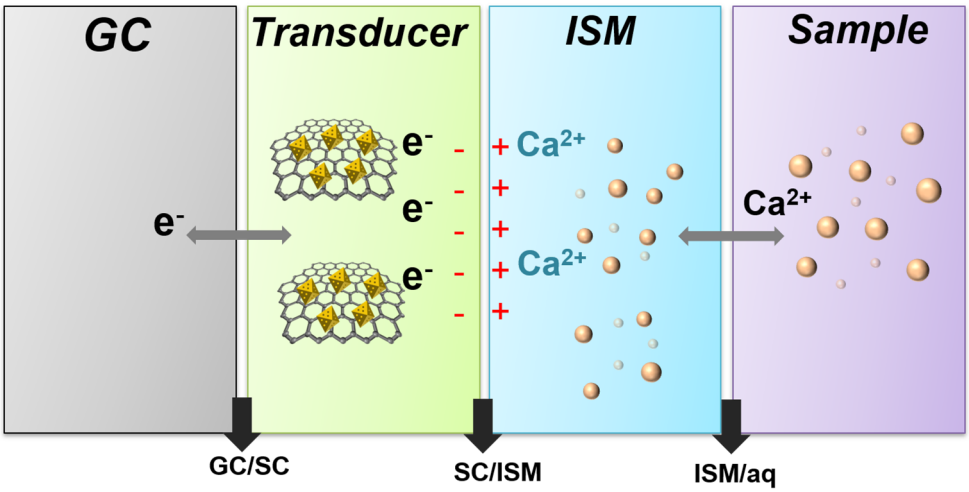


Figure 4. Transfer mechanism based on double electric layer (EDL) capacitor SC-ISE, including GC/SC, SC/ISM and ISM/aq interface three phase boundaries.

Studies have shown that water layers can lead to poor long-term potential stability. The electrode is tested in water layer in the presence or absence of solid contact layer material [37]. The electrodes were immersed in 0.1 M $CaCl_2$, 0.1 M NaCl and 0.1 M $CaCl_2$ respectively for water layer test, as shown in Figure 5a. The hydrophobicity of NH_2-MIL-125@rGO/Ca^{2+}-ISE prevented the obvious drift of the electrodes during the transition from NaCl solution to $CaCl_2$ solution. It is evident from Figure S7 that this low potential drift is due to the avoidance of water

layer accumulation at the SC/ISM interface, which indicates that the water film in NH_2-MIL-125@rGO/Ca^{2+}-ISE is negligible.

To further confirm the hydrophobicity of the composite materials, two water contact angle tests were conducted on NH_2-MIL-125 and NH_2-MIL-125@rGO. The results showed in Figure S10 indicate that the water contact angle of NH_2-MIL-125 was 96.40°, while that of NH_2-MIL-125@rGO increased to 116.56°, indicating that the introduction of rGO further enhanced the hydrophobicity of the material. This effectively inhibited the formation of the interfacial water layer between the solid contact layer and the ion-selective membrane, which was beneficial for reducing electrode potential drift and improving the long-term stability of the electrode.

Electrode potentials of Ca^{2+}-ISE, NH_2-MIL-125/Ca^{2+}-ISE, and NH_2-MIL-125@rGO/Ca^{2+}-ISE were measured in 0.1 M $CaCl_2$ for 12 h to assess long-term potential stability. As is shown in Figure 5b, the long-term potential shifts of Ca^{2+}-ISE, NH_2-MIL-125/Ca^{2+}-ISE and NH_2-MIL-125@rGO/Ca^{2+}-ISE were 12.85 ± 0.34 mV·h^{-1}, 4.13 ± 0.13 mV·h^{-1} and 66.7 ± 0.12 μV·h^{-1}, respectively (n = 3). The proposed NH_2-MIL-125@rGO/Ca^{2+}-ISE has very low long-term potential drift, which is lower than other Ca^{2+}-ISE. This can be attributed to the large double electric layer capacitance and high hydrophobicity of the composite, which enables fast ion-electron transduction.

Constant current chronopotentiometry was used to analyze the short-term potential stability of the potential sensor. (Figure 5c) The capacitance value was accurately obtained according to the formula: $\Delta E/\Delta t = I/C$, where I is the applied current (±1 nA), Δt is the applied current time, and C is the capacitance [38]. The potential drift ($\Delta E/\Delta t$) of NH_2-MIL-125@rGO/Ca^{2+}-ISE was only 4.5 ± 0.1 μV·s^{-1} (n = 3), which was much greater than that of NH_2-MIL-125/Ca^{2+}-ISE (18 μV·s^{-1}) and Ca^{2+}-ISM (792 μV·s^{-1}), and the calculated capacitance of NH_2-MIL-125@rGO/Ca^{2+}-ISE is 222 μF. The obtained capacitance is higher than SC-ISE most of other double-layer capacitor materials [18], redox capacitor materials [23] and mixed capacitor materials [39] transducers as shown in (Table S1). The results showed that the short-term potential stability and capacitance of Ca^{2+}-ISE are significantly improved when NH_2-MIL-125@rGO is introduced as the SC layer.

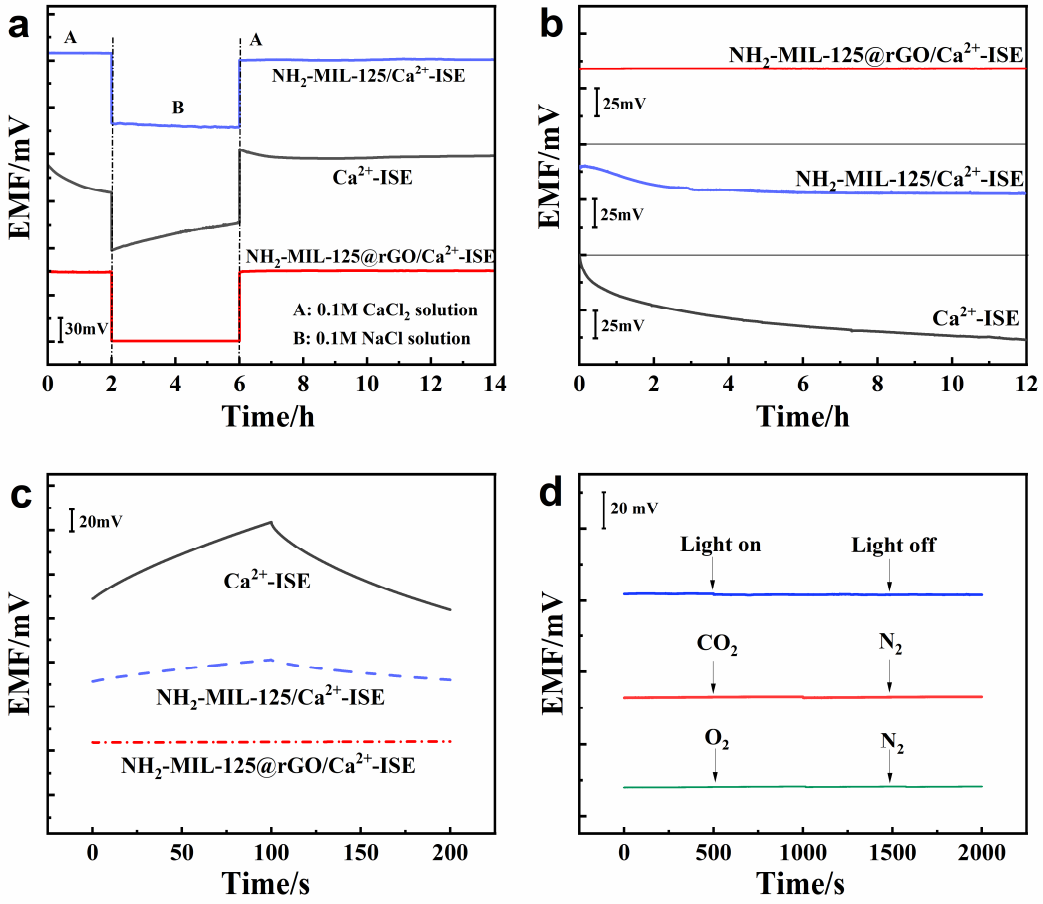


Figure 5. (**a**) Water layer tests for Ca^{2+}-ISE, NH_2-MIL-125/Ca^{2+}-ISE and NH_2-MIL-125@rGO/Ca^{2+}-ISE; (**b**) Long-term potential stability tests for Ca^{2+}-ISE NH_2-MIL-125/Ca^{2+}-ISE and NH_2-MIL-125@rGO/Ca^{2+}-ISE in 0.1 M $CaCl_2$; (**c**) Chronopotentiograms tests for Ca^{2+}-ISE NH_2-MIL-125/Ca^{2+}-ISE and NH_2-MIL-125@rGO/Ca^{2+}-ISE in 0.1 M $CaCl_2$; (**d**) NH_2-MIL-125@rGO/Ca^{2+}-ISE anti-interference (light and gas) test at 0.1 M $CaCl_2$.

The effects of light and gas on the electrodes were studied by monitoring the potentials of NH_2-MIL125@rGO/Ca^{2+}-ISE by turning on or off the light and bubbling N_2, CO_2 and O_2 in 1 mM $CaCl_2$ solution. No significant potential drift was observed in NH_2-MIL125@rGO/Ca^{2+}-ISE during measurement (Figure 5d). These results indicate that NH_2-MIL125@rGO/Ca^{2+}-ISE has excellent resistance to environmental disturbance.

The potential response test of SC-ISE was performed in $CaCl_2$ solution with a concentration range of 10^{-10}~10^{-1} M. As shown in Figure 6a,b, a potential response was observed over a linear range of 10^{-7}~10^{-1} M with a sensitivity of 23.96 mV·dec^{-1} (R^2 = 0.995) and a low detection limit of $10^{-7.2}$ M was calculated. The detection limit was determined from the potentiometric calibration curve using the intersection method. The Nernstian linear-response region and the low-concentration non-Nernstian region were separately fitted by linear regression, and the intersection of the two extrapolated lines was defined as the detection limit. The calculation results of Ca^{2+}-ISE are shown in Figure S5. The results show that the NH_2-MIL-125@rGO/Ca^{2+}-ISE does so even at lower concentrations. It can be seen that the detection limits are wider than other Ca^{2+}-ISE reported in Table S1 and Table S2. The excellent stability and sensitivity properties are attributed to the introduction of solid contact layer materials. The SC-ISE electrode was stored in 10^{-3} M $CaCl_2$ solution, and the potential potential response of the same SC-ISE to Ca^{2+} was continuously recorded over seven days. As shown in Figure S6, the detection limit and response slope do not change significantly, which proves that the electrode has good long-term potential stability.

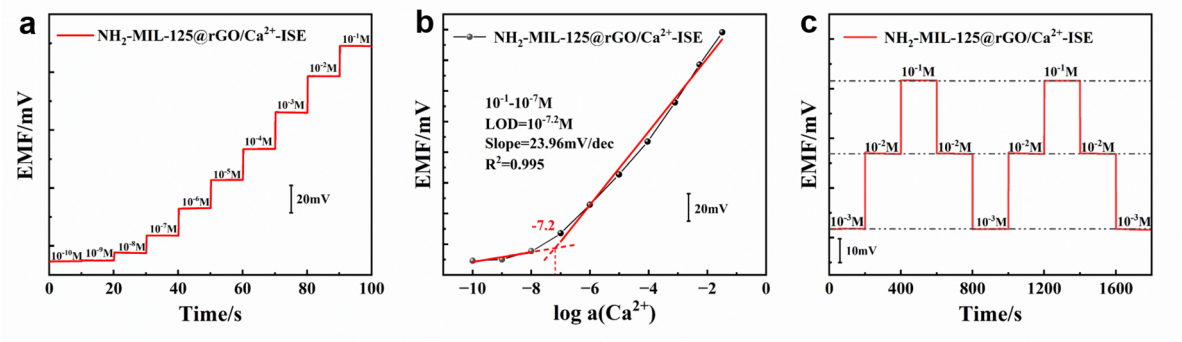


Figure 6. (**a**,**b**) Potential response and calibration curves of NH_2-MIL-125@rGO/Ca^{2+}-ISE to Ca^{2+} in the concentration range of 10^{-10}~10^{-1} M; (**c**) invertibility tests for NH_2-MIL-125@rGO/Ca^{2+}-ISE.

The electrode was repeatedly soaked in 10^{-3}~10^{-1} M $CaCl_2$ solution for 9 times to obtain reversibility, measure potential response, and record potential change curve. As can be seen from Figure 6c, when NH_2-MIL-125@rGO/Ca^{2+}-ISE is alternately measured in the three solutions, corresponding potential values can be maintained at different concentrations. Subsequently, reproducibility of Ca^{2+} ions was tested using five different NH_2-MIL-125@rGO/Ca^{2+}-ISE electrodes (Figure S8a,b). The stable potential values and calibration curve slope of 5 different NH_2-MIL-125@rGO/Ca^{2+}-ISE electrodes have good repeatability. The results show that the NH_2-MIL-125@rGO/Ca^{2+}-ISE electrode has excellent reversibility.

The selectivity of electrode was evaluated by separating solution method [40]. The selectivity coefficient was calculated as shown in Figure 7a. The selectivity coefficient of the prepared NH_2-MIL-125@rGO/Ca^{2+}-ISE for Na^+, K^+, Mg^{2+} and Fe^{3+} was measured, and the potential was measured in the solution of NaCl, KCl $MgCl_2$ and $FeCl_3$ at a concentration of 0.01 M. The measured primary and discriminant ions show close to Nernst responses. NH_2-MIL-125@rGO/Ca^{2+}-ISE shows high selectivity for interfering ions, and the selectivity coefficient is consistent with that reported for Ca^{2+}-ISE [41]. In addition, ions may penetrate the ISM into the SC layer, which may cause the electrode's potential response to be unstable. When different ionic solutions were added successively to the solution to be tested, compared with Ca^{2+}-ISE and NH_2-MIL125/Ca^{2+}-ISE, NH_2-MIL-125@rGO/Ca^{2+}-ISE did not detect significant potential drift (Figure 7b). It indicates that NH_2-MIL-125@rGO/Ca^{2+}-ISE has excellent excellent anti-ion interference performance.

In order to verify the reliability of the prepared NH_2-MIL-125@rGO/Ca^{2+}-ISE, the Ca^{2+} concentration in the actual milk sample was detected and analyzed, and a disposable NH_2-MIL-125@rGO/Ca^{2+}-ISE was set up to measure the calcium in the actual sample. The results of SPE/NH_2-MIL-125@rGO/Ca^{2+}-ISE and inductively coupled plasma mass spectrometry (ICP-MS) were compared to evaluate the feasibility of the electrode. As shown in Figure 7c, the accuracy of SPE/NH_2-MIL-125@rGO/Ca^{2+}-ISE and ICP-MS is basically the same. The solid-contact calcium ion selective electrode with NH_2-MIL-125@rGO as the ion-electron transduction layer has excellent analytical response performance.

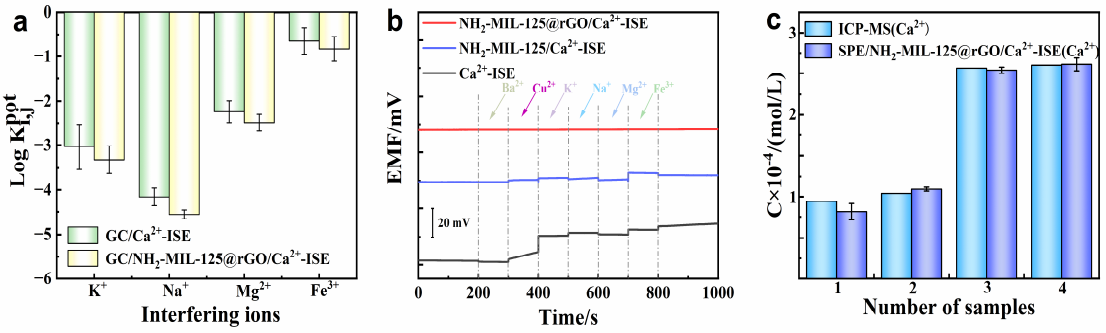


Figure 7. (**a**) Selective tests for NH_2-MIL-125@rGO/Ca^{2+}-ISE and Ca^{2+}-ISE; (**b**) Ion resistance tests for Ca^{2+}-ISE, NH_2-MIL-125/Ca^{2+}-ISE and NH_2-MIL-125@rGO/Ca^{2+}-ISE; (**c**) Comparison of NH_2-MIL-125@rGO/Ca^{2+}-ISE electrode and ICP-MS assay results for detection of Ca^{2+} concentration in four different milk samples labeled 1–4.

4. Conclusions

In summary, NH_2-MIL-125@rGO composites prepared by a simple solvothermal method have been successfully used to produce SC-Ca^{2+}-ISE. The high porosity and large specific surface area of the composite effectively increase the contact area between the transducer and ISM, which is conducive to reducing the interfacial resistance and promoting the ion-electron transfer ability. In addition, the prepared NH_2-MIL-125@rGO/Ca^{2+}-ISE has excellent potential stability, and the potential drift is not obvious. The electrode exhibits a wide linear activity range from 10^{-7} to 10^{-1} M with a detection limit of $10^{-7.2}$ M, demonstrating excellent Nernstian response and outstanding potential reproducibility. It is insensitive to light, gases and ions. The method has been successfully applied disposable screen printed electrode to the detection of actual milk samples which indicated reliable results compared with ICP-MS. We believe NH_2-MIL-125@rGO/Ca^{2+}-ISE has the potential for practical applications in milk calcium monitoring.

Supplementary Materials

The additional data and information can be downloaded at: https://media.sciltp.com/articles/others/26102 21452242206/eChem-26060268-SM.pdf. Figure S1. EDS and mass and atomic percentage elements of NH_2-MIL-125@rGO. Figure S2. Elemental mapping images C, N, O and Ti in the NH_2-MIL-125@rGO. Figure S3. (a) XPS spectra of NH_2-MIL-125 and (b,c) XPS spectra of N 1s and O 1s at NH_2-MIL-125; (d) XPS spectra of NH_2-MIL-125@rGO and (e,f) XPS spectra of N 1s and O 1s for NH_2-MIL-125@rGO. Figure S4. (a) Impedance spectra of Ca^{2+}-ISE, NH_2-MIL-125/Ca^{2+}-ISE and NH_2-MIL-125@rGO/Ca^{2+}-ISE in 0.1 M $CaCl_2$ aqueous solution. Insets represent the equivalent electrical circuits. Rs is the resistance of the solution. Rct is the volume resistance of ISM and the contact resistance between the SC/ISM interface, controlling the semi-circle diameter. CPE is double-layer capacitance. Z_w is the "classical" finite-length Warburg impedance identified with the linear portion of the impedance spectra that appears at the lower frequencies [1]; (b) Impedance spectra of rGO/Ca^{2+}-ISE and GO/Ca^{2+}-ISE. Figure S5. (a,b) Potential response and calibration curves of GC/Ca^{2+}-ISE to Ca^{2+} at concentrations ranging from 10^{-9}~10^{-1} M. Figure S6. Potential response test of Ca^{2+} for seven consecutive days by NH_2-MIL-125@rGO/Ca^{2+}-ISE. Figure S7. Aqueous test curves of (a) Ca^{2+}-ISE and (b) NH_2-MIL-125/Ca^{2+}-ISE and (c) NH_2-MIL-125@rGO/Ca^{2+}-ISE in 0.1 M $CaCl_2$ or 0.1 M NaCl solution (red lines are horizontal lines, The black line is the test line). Figure S8. (a) NH_2-MIL-125@rGO/Ca^{2+}-ISE electrode potential response diagram repeated 5 times in 10^{-1}~10^{-4} M $CaCl_2$ solution and (b) potential calibration curve. Figure S9. (a) TEM images of NH_2-MIL-125 and (b) NH_2-MIL-125@rGO. Figure S10. Water contact angle of (a)NH_2-MIL-125 and (b) NH_2-MIL-125@rGO. Table S1. Comparison of the potentiometric performance of the NH_2-MIL-125@rGO based Ca^{2+}-ISEs with the reported other materials Ca^{2+}-ISEs. Table S2. Detection limits comparison of Ca^{2+}-ISE based on NH_2-MIL-125@rGO with solid contact ion-selective electrodes constructed with other MOF's composites. Table S3. The best equivalent circuit and the corresponding parameters for the developed electrodes were as follows. References [42–46] are cited in supplementary materials.

Author Contributions

W.Z.: investigation, data curation, formal analysis, writing—original draft preparation; Y.F.: investigation, methodology, validation, data curation; Q.A.: conceptualization, methodology, supervision, funding acquisition, writing—review and editing; Z.S.: supervision, writing—review and editing; B.C.: supervision, writing—review

and editing; J.S.: supervision, project administration, writing—review and editing; L.N.: supervision, writing—review and editing. All authors have read and agreed to the published version of the manuscript and accept accountability for their respective contributions.

Funding

This work was supported by the National Natural Science Foundation of China (Grant No. 22434007), the Science and Technology Development Planning of Jilin Province (YDZJ202301ZYTS309) and the Science and Technology of Education Department of Jilin Province (JJKH20250486KJ).

Data Availability Statement

The data presented in this study are available on request from the corresponding author.

Conflicts of Interest

The authors declare no conflict of interest.

Use of AI and AI-Assisted Technologies

No AI tools were utilized for this paper.

References

1. Ratajczak, A.E.; Zawada, A.; Rychter, A.M.; et al. Milk and Dairy Products: Good or Bad for Human Bone? Practical Dietary Recommendations for the Prevention and Management of Osteoporosis. *Nutrients* **2021**, *13*, 1329. https://doi.org/10.3390/nu13041329.
2. Béni, Á.; Nagy, D.; Kapitány, S.; et al. Separation/Preconcentration of Chromium Species with Continuous Liquid-Liquid Extraction Device and Its Determination by AAS. *Microchem. J.* **2019**, *150*, 104077. https://doi.org/10.1016/j.microc.2019.104077.
3. Qin, L.M.; Yang, X.A.; Leng, D.; et al. Dual-Frequency Ultrasound Assisted-Enzyme Digestion Coupled with Atomic Fluorescence Spectrometry as a Green and Efficient Tool for Cadmium Detection in Rice Flour Samples. *Talanta* **2018**, *188*, 308–315. https://doi.org/10.1016/j.talanta.2018.06.007.
4. Tang, T.; Landis, W.; Blouin, S.; et al. Subcanalicular Nanochannel Volume Is Inversely Correlated with Calcium Content in Human Cortical Bone. *J. Bone Miner. Res.* **2023**, *38*, 313–325. https://doi.org/10.1002/jbmr.4753.
5. Zdrachek, E.A.; Bakker, E. Potentiometric Sensing. *Anal. Chem.* **2021**, *93*, 72–102. https://doi.org/10.1021/acs.analchem.0c04249.
6. Lyu, Y.; Gan, S.; Bao, Y.; et al. Solid-Contact Ion-Selective Electrodes: Response Mechanisms, Transducer Materials and Wearable Sensors. *Membranes* **2020**, *10*, 128. https://doi.org/10.3390/membranes10060128.
7. Kałuża, D.; Jaworska, E.; Mazur, M.; et al. Multiwalled Carbon Nanotubes–Poly(3-Octylthiophene-2,5-Diyl) Nanocomposite Transducer for Ion-Selective Electrodes: Raman Spectroscopy Insight into the Transducer/Membrane Interface. *Anal. Chem.* **2019**, *91*, 9010–9017. https://doi.org/10.1021/acs.analchem.9b01286.
8. Papp, S.; Bojtár, M.; Gyurcsányi, R.E.; et al. Potential Reproducibility of Potassium-Selective Electrodes Having Perfluorinated Alkanoate Side Chain Functionalized Poly(3,4-Ethylenedioxytiophene) as a Hydrophobic Solid Contact. *Anal. Chem.* **2019**, *91*, 9111–9118. https://doi.org/10.1021/acs.analchem.9b01587.
9. Jiang, C.; Li, X.; Yao, Y.; et al. Fully Written Flexible Potentiometric Sensor Using Two-Dimensional Nanomaterial-Based Conductive Ink. *Anal. Chem.* **2018**, *90*, 13088–13095. https://doi.org/10.1021/acs.analchem.8b04334.
10. Li, J.; Qin, W. A Freestanding All-Solid-State Polymeric Membrane Cu^{2+}-Selective Electrode Based on Three-Dimensional Graphene Sponge. *Anal. Chim. Acta* **2019**, *1068*, 11–17. https://doi.org/10.1016/j.aca.2019.04.003.
11. Li, J.; Qin, W. An Integrated All-Solid-State Screen-Printed Potentiometric Sensor Based on a Three-Dimensional Self-Assembled Graphene Aerogel. *Microchem. J.* **2020**, *159*, 105453. https://doi.org/10.1016/j.microc.2020.105453.
12. Zhang, Y.; Tang, Y.; Liang, R.; et al. Carbon-Based Transducers for Solid-Contact Calcium Ion-Selective Electrodes: Mesopore and Nitrogen-Doping Effects. *Membranes* **2022**, *12*, 903. https://doi.org/10.3390/membranes12090903.
13. Zhen, X.V.; Rousseau, C.R.; Bühlmann, P. Redox Buffer Capacity of Ion-Selective Electrode Solid Contacts Doped with Organometallic Complexes. *Anal. Chem.* **2018**, *90*, 11000–11007. https://doi.org/10.1021/acs.analchem.8b02595.
14. Jaworska, E.; Naitana, M.L.; Stelmach, E.; et al. Introducing Cobalt(II) Porphyrin/Cobalt(III) Corrole Containing Transducers for Improved Potential Reproducibility and Performance of All-Solid-State Ion-Selective Electrodes. *Anal. Chem.* **2017**, *89*, 7107–7114. https://doi.org/10.1021/acs.analchem.7b01027.
15. Jaworska, E.; Wójcik, M.; Kisiel, A.; et al. Gold Nanoparticles Solid Contact for Ion-Selective Electrodes of Highly Stable Potential Readings. *Talanta* **2011**, *85*, 1986–1989. https://doi.org/10.1016/j.talanta.2011.07.049.

16. Xu, J.; Sun, Z.; Li, F.; et al. Nitrogen-Doped Porous Carbon Derived from Zeolitic Imidazolate Framework-67 Strung into Necklace with Carbon Nanotubes for the Detection of Calcium at Ultralow Level. *J. Electrochem. Soc.* **2020**, *167*, 087512. https://doi.org/10.1149/1945-7111/ab91cb.
17. Mendecki, L.; Mirica, K.A. Conductive Metal–Organic Frameworks as Ion-to-Electron Transducers in Potentiometric Sensors. *ACS Appl. Mater. Interfaces* **2018**, *10*, 19248–19257. https://doi.org/10.1021/acsami.8b03956.
18. Shao, Y.; Yao, Y.; Jiang, C.; et al. Two-Dimensional MXene Nanosheets (Types $Ti_3C_2T_x$ and Ti_2CT_x) as New Ion-to-Electron Transducers in Solid-Contact Calcium Ion-Selective Electrodes. *Microchim. Acta* **2019**, *186*, 750. https://doi.org/10.1007/s00604-019-3878-7.
19. Bagheri, M.; Masoomi, M.Y. Quasi-Metal Organic Frameworks: Preparation, Applications and Future Perspectives. *Coord. Chem. Rev.* **2022**, *468*, 214643. https://doi.org/10.1016/j.ccr.2022.214643.
20. Meng, J.; Ashry, A.G.; Abou-Elyazed, A.S.; et al. Highly Efficient Visible-Light Photocatalysts: Bi_2O_3@TiO_2 Derived from Ti-MOFs for Eriochrome Black T Degradation: A Joint Experimental and Computational Study. *Catalysts* **2024**, *14*, 829. https://doi.org/10.3390/catal14110829.
21. Mokhtar, N.A.I.M.; Zawawi, R.M.; Khairul, W.M.; et al. Electrochemical and Optical Sensors Made of Composites of Metal–Organic Frameworks and Carbon-Based Materials. A Review. *Environ. Chem. Lett.* **2022**, *20*, 3099–3131. https://doi.org/10.1007/s10311-022-01403-2.
22. Shao, D.; Shi, J.; Zhang, J.; et al. Solvent Impedes CO_2 Cycloaddition on Metal–Organic Frameworks. *Chem. Asian J.* **2018**, *13*, 386–389. https://doi.org/10.1002/asia.201701706.
23. Li, Y.; Li, J.; Qin, W. Solid-Contact Polymeric Membrane Ion-Selective Electrodes Based on Electrodeposited $NiCo_2S_4$ Nanosheet Arrays. *Talanta* **2023**, *251*, 123797. https://doi.org/10.1016/j.talanta.2022.123797.
24. Jin, J.; Kim, J.P.; Wan, S.; et al. Hierarchical Pore Enhanced Adsorption and Photocatalytic Performance of Graphene Oxide/Ti-Based Metal-Organic Framework Hybrid for Toluene Removal. *Appl. Catal. B Environ.* **2022**, *317*, 121751. https://doi.org/10.1016/j.apcatb.2022.121751.
25. Wang, J.; Yu, Z.; Zhu, X.; et al. A Super-Hydrophilic NH_2-MIL-125 Composite Film with Dopamine-Modified Graphene Oxide Is Used for Water Treatment. *New J. Chem.* **2022**, *46*, 13303–13314. https://doi.org/10.1039/d2nj02181a.
26. Shu, Z.; Zou, Y.; Wu, X.; et al. NH_2-MIL-125(Ti)/Reduced Graphene Oxide Enhanced Electrochemical Detection of Fenitrothion in Agricultural Products. *Foods* **2023**, *12*, 1534. https://doi.org/10.3390/foods12071534.
27. Li, X.; Le, Z.; Chen, X.; et al. Graphene Oxide Enhanced Amine-Functionalized Titanium Metal Organic Framework for Visible-Light-Driven Photocatalytic Oxidation of Gaseous Pollutants. *Appl. Catal. B Environ.* **2018**, *236*, 501–508. https://doi.org/10.1016/j.apcatb.2018.05.052.
28. Yuan, X.; Wang, H.; Wu, Y.; et al. One-Pot Self-Assembly and Photoreduction Synthesis of Silver Nanoparticle-Decorated Reduced Graphene Oxide/MIL-125(Ti) Photocatalyst with Improved Visible Light Photocatalytic Activity. *Appl. Organomet. Chem.* **2016**, *30*, 289–296. https://doi.org/10.1002/aoc.3430.
29. Pimenta, M.A.; Dresselhaus, G.; Dresselhaus, M.S.; et al. Studying Disorder in Graphite-Based Systems by Raman Spectroscopy. *Phys. Chem. Chem. Phys.* **2007**, *9*, 1276–1290. https://doi.org/10.1039/b613962k.
30. Bagri, A.; Mattevi, C.; Acik, M.; et al. Structural Evolution during the Reduction of Chemically Derived Graphene Oxide. *Nat. Chem.* **2010**, *2*, 581–587. https://doi.org/10.1038/nchem.686.
31. Wang, Q.; Wang, G.; Liang, X.; et al. Supporting Carbon Quantum Dots on NH_2-MIL-125 for Enhanced Photocatalytic Degradation of Organic Pollutants under a Broad Spectrum Irradiation. *Appl. Surf. Sci.* **2019**, *467–468*, 320–327. https://doi.org/10.1016/j.apsusc.2018.10.165.
32. Wang, H.; Yuan, X.; Wu, Y.; et al. Facile Synthesis of Amino-Functionalized Titanium Metal-Organic Frameworks and Their Superior Visible-Light Photocatalytic Activity for Cr(VI) Reduction. *J. Hazard. Mater.* **2015**, *286*, 187–194. https://doi.org/10.1016/j.jhazmat.2014.11.039.
33. Paczosa-Bator, B. Ion-Selective Electrodes with Superhydrophobic Polymer/Carbon Nanocomposites as Solid Contact. *Carbon* **2015**, *95*, 879–887. https://doi.org/10.1016/j.carbon.2015.09.006.
34. Lai, C.Z.; Joyer, M.M.; Fierke, M.A.; et al. Subnanomolar Detection Limit Application of Ion-Selective Electrodes with Three-Dimensionally Ordered Macroporous (3DOM) Carbon Solid Contacts. *J. Solid State Electrochem.* **2009**, *13*, 123–128. https://doi.org/10.1007/s10008-008-0579-2.
35. Xu, J.; Jia, F.; Li, F.; et al. Simple and Efficient Synthesis of Gold Nanoclusters and Their Performance as Solid Contact of Ion Selective Electrode. *Electrochim. Acta* **2016**, *222*, 1007–1012. https://doi.org/10.1016/j.electacta.2016.11.069.
36. Hu, J.; Zou, X.U.; Stein, A.; et al. Ion-Selective Electrodes with Colloid-Imprinted Mesoporous Carbon as Solid Contact. *Anal. Chem.* **2014**, *86*, 7111–7118. https://doi.org/10.1021/ac501633r.
37. Fibbioli, M.; Morf, W.E.; Badertscher, M.; et al. Potential Drifts of Solid-Contacted Ion-Selective Electrodes Due to Zero-Current Ion Fluxes through the Sensor Membrane. *Electroanalysis* **2000**, *12*, 1286–1292.
38. Bobacka, J. Potential Stability of All-Solid-State Ion-Selective Electrodes Using Conducting Polymers as Ion-to-Electron Transducers. *Anal. Chem.* **1999**, *71*, 4932–4937. https://doi.org/10.1021/ac990497z.

39. Chai, D.; Sun, Y.; Li, Z.; et al. A Novel Inorganic Redox Buffer of R-GO/Ag@AgCl/TMMCl Utilized as an Effective Ion-to-Electron Transducer for a Solid Contact Calcium Ion-Selective Electrode. *Sens. Actuators B Chem.* **2022**, *367*, 132055. https://doi.org/10.1016/j.snb.2022.132055.
40. Bakker, E. Determination of Improved Selectivity Coefficients of Polymer Membrane Ion-Selective Electrodes by Conditioning with a Discriminated Ion. *J. Electrochem. Soc.* **1996**, *143*, L83–L85. https://doi.org/10.1149/1.1836608.
41. Li, Y.; Li, J.; Qin, W. All-Solid-State Polymeric Membrane Ion-Selective Electrodes Based on $NiCo_2S_4$ as a Solid Contact. *Anal. Chem.* **2022**, *94*, 3574–3580. https://doi.org/10.1021/acs.analchem.1c04748.
42. Sundfors, F.; Bobacka, J. EIS Study of the Redox Reaction of $Fe(CN)_6^{3-/4-}$ at Poly(3,4-Ethylenedioxythiophene) Electrodes: Influence of DC Potential and cOx:cRed Ratio. *J. Electroanal. Chem.* **2004**, *572*, 309–316. https://doi.org/10.1016/j.jelechem.2003.12.013.
43. Yin, T.; Li, J.; Qin, W. An All-Solid-State Polymeric Membrane Ca^{2+}-Selective Electrode Based on Hydrophobic Alkyl-Chain-Functionalized Graphene Oxide. *Electroanalysis* **2017**, *29*, 821–827. https://doi.org/10.1002/elan.201600383.
44. Jiang, C.; Yao, Y.; Cai, Y.; et al. All-Solid-State Potentiometric Sensor Using Single-Walled Carbon Nanohorns as Transducer. *Sens. Actuators B Chem.* **2019**, *283*, 284–289. https://doi.org/10.1016/j.snb.2018.12.040.
45. Zeng, X.; Qin, W. A Solid-Contact Ca^{2+}-Selective Electrode Based on an Inorganic Redox Buffer of Ag@AgCl/1-Tetradecyl-3-Methylimidazolium Chloride as Ion-to-Electron Transducer. *Talanta* **2020**, *209*, 120570. https://doi.org/10.1016/j.talanta.2019.120570.
46. Kaur, N.; Kaur, J.; Badru, R.; et al. BGO/AlFu MOF Core Shell Nano-Composite Based Bromide Ion-Selective Electrode. *J. Environ. Chem. Eng.* **2020**, *8*, 104375. https://doi.org/10.1016/j.jece.2020.104375.